Applied Radiation and Isotopes 148 (2019) 232–239

Contents lists available at ScienceDirect

Applied Radiation and Isotopes

journal homepage: www.elsevier.com/locate/apradiso

Mass energy absorption coefficients and energy responses of magnesium tetraborate dosimeters for 0.02 MeV to 20 MeV photons using Monte Carlo simulations

Luiza F. Souza[a,*], William S. Santos[a,b], Walmir Belinato[c], Rogerio M.V. Silva[d], Linda V.E. Caldas[a], Divanizia N. Souza[d]

[a] Instituto de Pesquisas Energéticas e Nucleares, Comissão Nacional de Energia Nuclear, IPEN-CNEN/SP, São Paulo, SP, Brazil
[b] Instituto de Física, Universidade Federal de Uberlândia, Uberlândia, MG, Brazil
[c] Departamento de Ensino, Instituto Federal de Educação, Ciência e Tecnologia da Bahia, Vitória da Conquista, BA, Brazil
[d] Departamento de Física, Universidade Federal de Sergipe (UFS), São Cristóvão, SE, Brazil

HIGHLIGHTS

- μ_{en}/ρ and the energy dependence of doped and undoped MgB_4O_7 were evaluated.
- Comparison with standard TLD and ICRU tissue data was performed.
- The values obtained from simulations were compared with theoretical calculations.
- An increase in the energy dependence of MgB4O7 was observed in the low energy range.

ARTICLE INFO

Keywords:
Thermoluminescence dosimetry
Monte Carlo
Energy response
Mass energy absorption coefficient

ABSTRACT

Thermoluminescence dosimeters containing boron, such as magnesium tetraborate (MgB_4O_7), are of interest because of their very high sensitivity, near tissue-equivalent absorption coefficients, low cost, easy handling, and very large linearity range for absorbed dose. Another important parameter that should be considered when working with thermoluminescent dosimeter (TLD) is the mass energy absorption coefficient (μ_{en}/ρ), which is a close approximation to the energy available for production of chemical, biological and other effects associated with exposure to ionizing radiation, therefore important in estimating dose in medical and health physics. In this study the mass energy absorption coefficients and energy responses of undoped and some doped magnesium tetraborates were calculated by Monte Carlo N-particle transport code for a range of photon energies between 20 keV and 20 MeV. The calculated parameters for MgB_4O_7, MgB_4O_7:Dy and MgB_4O_7:Dy,Li were evaluated in comparison with standard TLDs as Al_2O_3:C and TLD-100 (LiF: Mg, Ti) and ICRU tissue data. The influence of the dopant concentration in the MgB_4O_7 matrix on the energy dependence of TLD was also investigated. The analyses indicated a good agreement between the simulations and theoretical calculations. The μ_{en}/ρ and energy dependence of the materials are higher in the low energy range ($E < 100$ keV), which is related to the high probability of interaction between radiation and matter due to photoelectric absorption. With regard to the influence of dysprosium concentration in the MgB_4O_7 matrix an increase in the energy dependence of MgB_4O_7 for higher concentrations of dopants was observed in the low energy range.

1. Introduction

Many types of thermoluminescent (TL) materials are used as radiation detectors in different fields, including the medical applications, industry, environmental monitoring, and space research (Chen and McKeever, 1997; McKeever, 1985). The major advantages of thermoluminescent dosimeters are their wide useful dose range, small physical size, reusability and many of them are tissue equivalent (Bos, 2001; Attix, 1991). For a thermoluminescent dosimeter (TLD) to be used as a tissue substitute or tissue-equivalent dosimeter for photon interaction, the absorption and scattering radiation obtained for its constituent material must be very similar to that experienced by the soft

* Corresponding author.
E-mail address: divanizi@ufs.br (D.N. Souza).

https://doi.org/10.1016/j.apradiso.2019.04.015
Received 7 August 2018; Received in revised form 8 March 2019; Accepted 10 April 2019
Available online 13 April 2019

tissue under similar conditions (Knoll, 2010; Turner, 1995; Manjunatha, 2014a, 2014b, 2016). The use of a tissue-equivalent dosimeter is crucial, especially when low and medium energies are employed, such as in brachytherapy and diagnostic procedures (Bos, 2001). Also, in radiotherapy practices it becomes important when it goes towards out-of-field measurements. This is because the deposition of the radiation undergoes contributions related to leakage radiation from the head of the treatment machine and scatter radiation from the collimator system or inside the phantom or patient, which generally is composed by lower energy spectrum (< 100 keV) and so low energy-dependent detector is most required.

A common way to compare the interaction of radiation with soft tissue and a tissue-equivalent material is to consider the mass energy absorption coefficient (μ_{en}/ρ) or the effective atomic number (Z_{eff}) (Kumar and Reddy, 1997; Manjunatha and Rudraswamy, 2011, 2012, 2013). The μ_{en}/ρ is a fair approximation to the amount of photon energy available for the production of chemical, biological, and other effects associated with exposure to ionizing radiation and therefore it is useful for estimating the absorbed dose in medical and health physics (ICRU-33, 1980; Hubbell, 2000). Another important parameter to analyze in a TLD detector is the photon energy response, which is directly correlated to μ_{en}/ρ (Horowitz, 1981). Information on energy response is helpful in selecting the filter or any other energy correction method for a TLD material, and it can also define its applicability.

TLDs containing the element boron, such as lithium (e.g. LiB_4O_7) and magnesium borates (e.g. MgB_4O_7), are of interest due to their near tissue equivalence, low-cost raw materials, linear behavior of the dose response, from low to high doses, and Z_{eff} close to that of human tissue (approximately 8.4). They are also three to seven times more sensitive than the commercial TLD-100 (Yukihara et al., 2013, 2014), and are suited for applications in personal dosimetry, radiation therapy and even for applications that involve very high doses (Prokic, 1983, 1986, 2000, 2007; Prokic and Botter, 1993; Yukihara and McKeever, 2011).

With regard to the theoretical aspect, there are very few discussions about μ_{en}/ρ and the energy response of MgB_4O_7 compounds. Only few considerations were cited by Hubbell (1982) and Hubbell and Seltzer (1995), but due to the limited knowledge about MgB_4O_7 during that period, the authors did not consider the role of dopants in the MgB_4O_7 matrix, their influence on μ_{en}/ρ and the energy response of the compound in question. Nowadays, some studies have been carried out to understand the luminescent processes resulting from the interaction of ionizing radiation with this material (Yukihara et al., 2017; Souza et al., 2014, 2015; Paluch-Ferszt et al., 2014), and it is already known that the dopant chosen or its concentration in the matrix can change the μ_{en}/ρ value of the detector, but still no further discussion was found for this matrix and its main dopants.

Therefore, the novelty of this work consisted in describing the roles of the dopant (dysprosium) and codopant (lithium) in the μ_{en}/ρ and the energy response of the matrix of MgB_4O_7. Both parameters are important for radiation dosimetry and should be taken into account when TLDs are used for clinical applications.

The μ_{en}/ρ and energy responses of magnesium tetraborates (MgB_4O_7, MgB_4O_7:Dy and MgB_4O_7:Dy,Li) were fully described upon different photon energies, from 0.02 MeV up to 20 MeV, via simulations using Monte Carlo N-particle transport code, and the results were compared with those from theoretical calculations using the data from Hubbell and Seltzer (1995). To consolidate the analyses, the simulations and calculations were also performed for the ICRU tissue and for the standard commercial TLD, such as Al_2O_3:C and TLD-100; all the results were compared to those obtained by Harder and Hermann (1985).

The main advantage of using computational simulations is the possibility of creating many scenarios for a wide variety of radiation beams, which is impossible in most cases through calculations or experimental setups (Harder and Hermann, 1985; Singh and Badiger, 2013; Pelowitz, 2011; Hossain and Wagiran, 2012; Mobit et al., 1998; Wang et al., 2004). Such simulation allows predicting also the influence of the incorporation of different materials or of radiation beams in a certain scenario. Another advantage is that computational simulations usually provide results faster than experimental analyses. However, the simulation will produce results for any input parameters even if any of them are incorrect. The lack of accurate knowledge of the geometry of the problem and on physical-chemical characteristics of the materials of interest may introduce some uncertainties that are difficult to assess, leading to incorrect results, and these aspects were also taken into account in the present analyses.

2. Material and methods

2.1. Monte Carlo simulations

Using MCNPX Monte Carlo code, it was possible to simulate the photon transport including photoelectric absorption with the possibility of K- and L-shell fluorescent emissions or Auger electron emission, coherent and incoherent scattering, and pair production. The interactions during the photon and electron transports were based on ENDF/B-VI8 cross-section libraries. In this study, the values of photon and electron cut-off energies, cross-sections, types of interaction, and variance reduction techniques were kept as MCNPX default values.

At the simulations, the dosimeters were placed on a thin plastic holder (1 mm depth) and were irradiated with a source to surface distance of 100 cm, as shown in Fig. 1. All the simulations were done using the same set-up, regardless of the detectors used (MgB_4O_7; MgB_4O_7:Dy; MgB_4O_7:Dy,Li; TLD-100, and Al_2O_3:C); the point source emitted radiation isotropically within a solid angle that irradiates a 10 cm × 10 cm field size. In Fig. 1 also is shown the direction and distribution of photons between the source and the TLDs.

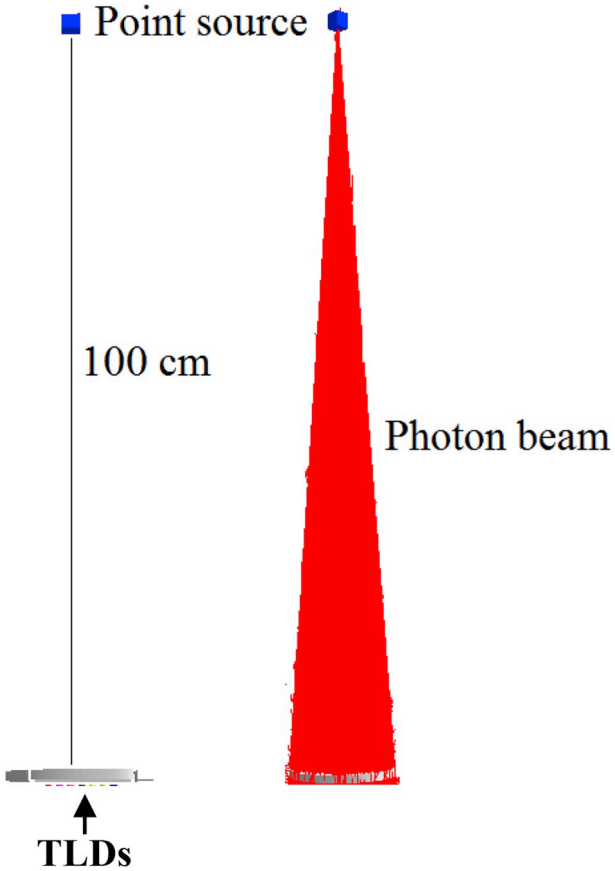

Fig. 1. Illustration showing the TLDs positioned under the source and the photon beam emitting radiation isotropically at a given solid angle.

Table 1
Density and effective atomic number (Z_{eff}) of the materials used in the present work. The Z_{eff} of the TL materials is calculated as a weighted mean value of the atomic number of the individual elements of each material (Bos, 2001).

Material	Z_{eff}	Density (g/cm^3)
ICRU Tissue	7.35	1.00
LiF:Mg,Ti (TLD-100)	8.31	2.64
Al_2O_3:C	11.28	3.85
MgB_4O_7	8.43	2.42

The simulations and calculations were performed for thirteen different energies, ranging from 0.02 MeV up to 20 MeV. For lower energies (≤0.08 MeV) small sub steps were used (e.g. 0.01 MeV) and for higher energies (≥0.08 MeV), the sub steps were greater (e.g. 1 MeV).

The typical CPU time for transporting 100 million histories varied between one hour (20 keV photon energy) and two hours (20 MeV photon energy). Photon transport simulations for 29 photon energy and six types of TLD (a total of 324 cases) were undertaken. The simulations were performed on a computer with a core i7 processor and 16 GB of RAM. Overall, the precision of the results was satisfactory considering the complex nature of the problem. All the uncertainties of simulations were below 1%.

For the simulations the Z_{eff} and density of the detectors were taken into account. In Table 1 are shown the respective characteristics of the TLDs evaluated and of the ICRU tissue. Among all the MgB_4O_7 (doped and undoped) samples described, the characteristics of the undoped MgB_4O_7 crystalline matrix were included in the table, once that no significant change in Z_{eff} and density is expected for the matrices thereof containing the dopants in proportions employed in this work.

2.2. Mass energy absorption coefficient (μ_{en}/ρ)

The mass energy absorption coefficient (μ_{en}/ρ) is the proportion of initial photon energy that is locally transferred to the material through ionization and excitation (Bos, 2001). By definition, μ_{en}/ρ is the product of the mass energy-transfer coefficient, μ_{tr}/ρ (cm^2/g), and (1 – g), where g is the fraction of the energy of the secondary charged particle that is lost to Bremsstrahlung interactions in the material. For theoretical calculations, the μ_{en}/ρ of a compound was performed using the mixture rule that is described by Equation (1):

$$\left(\frac{\mu_{en}}{\rho}\right)_{theory} = \sum_{i}^{n} w_i \left(\frac{\mu_{en}}{\rho}\right)_i = \sum_{i}^{n} w_i \left(\frac{\mu_{en}}{\rho}\right)_i \left(\frac{\mu_{en}}{\rho}\right)_{comp} = \sum_{i}^{n} w_i \left(\frac{\mu_{en}}{\rho}\right)_i \quad (1)$$

where W_i is the weight proportion for each element of the composite, and $(\mu_{en}/\rho)_i$ is the mass energy-absorption coefficient of the i th element (Manjunatha, 2016; Hubbell, 1982). The theoretical values of $(\mu_{en}/\rho)_i$ were taken from the compilation of Hubbell and Seltzer (1995), which is available on the NIST website. Table 2 shows the TLDs and ICRU tissue compositions and the respective weight fractions of each element in the compounds. For doped MgB_4O_7 detectors, the $(\mu_{en}/\rho)_i$ values of Dy or Li, were added in the mixture role [Equation (1)].

For the MCNPX simulations, the μ_{en}/ρ, represented by $(\mu_{en}/\rho)_{MCNPX}$ is the energy deposited in a TLD through energy fluence. The simulated macroscopic quantities, such as deposited energy, particle flow and energy flux, are computed by means of tallies. The MCNPX code provides seven standard tally types (Pelowitz, 2011). Here, the tallies F6 (MeV/g/particle) and *F4 (MeV/cm^2/particle) were used, representing the energy deposited in the material, per particle emitted by the source, and the energy fluency, respectively (Equation (2)).

$$\left(\frac{\mu_{en}}{\rho}\right)_{MCNPX} = \frac{F6\left(\frac{MeV}{\frac{g}{particle}}\right)}{F4\left(\frac{MeV}{\frac{cm^2}{particle}}\right)} f(E) = \frac{F6(MeV/g)}{*F4(MeV/cm^2)} \quad (2)$$

where $(\mu_{en}/\rho)_{MCNPX}$, represents the μ_{en}/ρ of TLD, for any given photon energy, in cm^2/g, achieved via Monte Carlo simulations.

2.3. Relative energy response

As described by Attix (1991), the energy response of a homogeneous dosimeter is estimated by the μ_{en}/ρ ratio of the dosimeter and a reference material. In this work, the reference material was the ICRU tissue, due to its similarity with the water density (1 g/cm^3), which is the main component of human tissue (70%) (Manjunatha and Rudraswamy, 2013; ICRU-33, 1980; Hubbell, 2000; Harder and Hermann, 1985). The relative energy response for the tetraborates (MgB_4O_7, MgB_4O_7:Dy, MgB_4O_7:Dy,Li), Al_2O_3:C, and TLD-100, from 0.02 MeV to 20 MeV, was calculated using Equation (3):

$$S(E)_{theory} = \left[\frac{\left(\mu_{en}/\rho\right)_{TLD.}}{\left(\mu_{en}/\rho\right)_{ref.}}\right] \quad (3)$$

where $S(E)_{theory}$ is the relative energy response of the TLD, the $(\mu_{en}/\rho)_{TLD.}$ and $(\mu_{en}/\rho)_{ref.}$ are the μ_{en}/ρ obtained by theoretical calculations (Eq. (1)), for the composite (TLDs) and the ICRU tissue, respectively.

For the simulations, 232 entry files were executed in the MNCPX code with each one containing the same information (e.g. chemical and physical characteristics of the dosimeter, irradiation geometry, photon source configuration, and particle numbers), except the photon energy. Equation (4) was used to obtain the energy response:

$$S(E)_{MCNPX} = \left[\frac{\left(\mu_{en}/\rho\right)_{TLD.}}{\left(\mu_{en}/\rho\right)_{ref.}}\right] \qquad S(E) = \frac{f(E)}{f(E)ref} \quad (4)$$

where $S(E)_{MCNPX}$ is the relative energy response for the TLD, $(\mu_{en}/\rho)_{TLD.}$ and $(\mu_{en}/\rho)_{ref.}$ are the simulated μ_{en}/ρ (Equation (2)) for the TLDs and ICRU tissue, respectively.

2.4. Dopant concentrations in the MgB_4O_7 matrix

To evaluate the effects of dopant concentrations in the energy

Table 2
Weight fraction of each element in the materials used in the present study (Bos, 2001; Hubbell and Seltzer, 1995).

Material	Element weight fraction in %										
	H	Li	B	C	N	O	F	Mg	Al	Ti	Dy
ICRU Tissue	$1.01.10^1$			$1.11.\ 10^1$	$2.60.10^0$	$7.62.\ 10^1$					
TLD-100 (LiF:Mg,Ti)		$2.65.\ 10^1$					$7.34.\ 10^1$	$2.20.10^{-4}$		$1.00.10^{-4}$	
Al_2O_3				$5.00.10^{-1}$		$4.71.\ 10^1$			$5.24.10^1$		
MgB_4O_7			$2.25.\ 10^1$			$6.36.\ 10^1$		$13.9.\ 10^1$			
MgB_4O_7:Dy			$2.24.\ 10^1$			$6.33.10^1$		$13.8.\ 10^1$			$5.00.10^{-1}$
MgB_4O_7:Dy,Li		$1.00.10^{-1}$	$2.24.\ 10^1$			$6.33.\ 10^1$		$13.7.\ 10^1$			$5.00.10^{-1}$

Table 3
Mass energy absorption coefficients μ_{en}/ρ (cm^2/g) with the statistical uncertainty (type A, σ_A) simulated by MCNPX for standard dosimeters, Al_2O_3:C and TLD-100 (LiF:Mg,Ti); magnesium borates, MgB_4O_7, MgB_4O_7:Dy, and MgB_4O_7:Dy,Li; and ICRU tissue.

MeV	Result	σ_A	Result	σ_A	Result	σ_A	Result	σ_A	Result	σ_A	Result	σ_A
Energy	Al_2O_3:C		TLD-100 (LiF:Mg,Ti)		MgB_4O_7		MgB_4O_7:Dy (0.5%)		MgB_4O_7:Dy,Li		ICRU tissue	
0.02	1.692	$7.000.10^{-3}$	0.651	$4.000.10^{-3}$	0.744	$2.000.10^{-3}$	0.967	$3.000.10^{-3}$	0.968	$3.000.10^{-3}$	0.510	$2.041.10^{-3}$
0.03	0.481	$2.000.10^{-3}$	0.183	$1.000.10^{-3}$	0.210	$6.956.10^{-4}$	0.285	$9.707.10^{-4}$	0.285	$9.698.10^{-4}$	0.146	$5.704.10^{-4}$
0.04	0.201	$8.043.10^{-4}$	0.079	$4.525.10^{-4}$	0.090	$3.003.10^{-4}$	0.124	$4.115.10^{-4}$	0.125	$4.111.10^{-4}$	0.066	$2.579.10^{-4}$
0.05	0.106	$4.255.10^{-4}$	0.045	$2.605.10^{-4}$	0.051	$1.712.10^{-4}$	0.070	$2.382.10^{-4}$	0.071	$2.380.10^{-4}$	0.041	$1.587.10^{-4}$
0.06	0.066	$2.676.10^{-4}$	0.032	$1.849.10^{-4}$	0.036	$1.163.10^{-4}$	0.060	$2.125.10^{-4}$	0.061	$2.124.10^{-4}$	0.031	$1.211.10^{-4}$
0.08	0.038	$1.536.10^{-4}$	0.023	$1.340.10^{-4}$	0.026	$8.366.10^{-5}$	0.042	$1.384.10^{-4}$	0.042	$1.383.10^{-4}$	0.026	$9.718.10^{-5}$
0.1	0.030	$1.172.10^{-4}$	0.022	$1.248.10^{-4}$	0.024	$7.689.10^{-5}$	0.034	$1.125.10^{-4}$	0.034	$1.124.10^{-4}$	0.025	$9.567.10^{-5}$
0.2	0.027	$1.029.10^{-4}$	0.024	$1.391.10^{-4}$	0.026	$8.162.10^{-5}$	0.028	$8.751.10^{-5}$	0.028	$8.749.10^{-5}$	0.029	$1.117.10^{-5}$
0.3	0.028	$1.081.10^{-4}$	0.027	$1.490.10^{-4}$	0.028	$8.741.10^{-5}$	0.029	$8.946.10^{-5}$	0.028	$8.947.10^{-5}$	0.032	$1.203.10^{-4}$
0.4	0.029	$1.107.10^{-4}$	0.027	$1.531.10^{-4}$	0.028	$8.977.10^{-5}$	0.029	$9.073.10^{-5}$	0.029	$9.072.10^{-5}$	0.033	$1.237.10^{-4}$
0.5	0.028	$1.112.10^{-4}$	0.027	$1.513.10^{-4}$	0.029	$9.034.10^{-5}$	0.029	$9.086.10^{-5}$	0.029	$9.086.10^{-5}$	0.033	$1.245.10^{-4}$
0.6	0.029	$1.107.10^{-4}$	0.027	$1.506.10^{-4}$	0.029	$8.993.10^{-5}$	0.029	$9.025.10^{-5}$	0.029	$9.024.10^{-5}$	0.032	$1.240.10^{-4}$
0.8	0.028	$1.095.10^{-4}$	0.026	$1.471.10^{-4}$	0.028	$8.787.10^{-5}$	0.029	$8.801.10^{-5}$	0.028	$8.799.10^{-5}$	0.032	$1.213.10^{-4}$
1	0.027	$1.047.10^{-4}$	0.026	$1.424.10^{-4}$	0.027	$8.507.10^{-5}$	0.027	$8.513.10^{-5}$	0.027	$8.512.10^{-5}$	0.031	$1.174.10^{-4}$
1.25	0.026	$1.000.10^{-4}$	0.025	$1.361.10^{-4}$	0.026	$8.134.10^{-5}$	0.026	$8.136.10^{-5}$	0.026	$8.135.10^{-5}$	0.029	$1.122.10^{-4}$
1.5	0.025	$9.570.10^{-5}$	0.023	$1.312.10^{-4}$	0.025	$7.776.10^{-5}$	0.0251	$7.78.10^{-5}$	0.025	$7.780.10^{-5}$	0.028	$1.072.10^{-4}$
2	0.023	$8.849.10^{-5}$	0.022	$1.201.10^{-4}$	0.023	$7.175.10^{-5}$	0.023	$7.176.10^{-5}$	0.023	$7.175.10^{-5}$	0.026	$1.072.10^{-4}$
3	0.020	$7.857.10^{-5}$	0.019	$1.056.10^{-4}$	0.020	$6.323.10^{-5}$	0.020	$6.328.10^{-5}$	0.020	$6.327.10^{-5}$	0.023	$9.880.10^{-5}$
4	0.019	$7.258.10^{-5}$	0.017	$9.648.10^{-5}$	0.018	$5.784.10^{-5}$	0.018	$5.795.10^{-5}$	0.019	$5.794.10^{-5}$	0.021	$8.654.10^{-5}$
5	0.018	$6.869.10^{-5}$	0.016	$9.023.10^{-5}$	0.017	$5.419.10^{-5}$	0.017	$5.435.10^{-5}$	0.017	$5.434.10^{-5}$	0.019	$7.855.10^{-5}$
6	0.017	$6.609.10^{-5}$	0.015	$8.585.10^{-5}$	0.016	$5.162.10^{-5}$	0.018	$5.182.10^{-5}$	0.016	$5.181.10^{-5}$	0.018	$7.298.10^{-5}$
8	0.016	$6.313.10^{-5}$	0.014	$8.025.10^{-5}$	0.015	$4.842.10^{-5}$	0.016	$4.869.10^{-5}$	0.016	$4.869.10^{-5}$	0.017	$6.597.10^{-5}$
10	0.016	$6.172.10^{-5}$	0.014	$7.703.10^{-5}$	0.015	$4.662.10^{-5}$	0.015	$4.696.10^{-5}$	0.015	$4.695.10^{-5}$	0.016	$6.191.10^{-5}$
15	0.016	$6.091.10^{-5}$	0.013	$7.345.10^{-5}$	0.014	$4.471.10^{-5}$	0.014	$4.518.10^{-5}$	0.015	$4.517.10^{-5}$	0.015	$6.052.10^{-5}$
20	0.016	$6.051.10^{-5}$	0.013	$7.345.10^{-5}$	0.014	$4.234.10^{-5}$	0.013	$4.236.10^{-5}$	0.014	$4.345.10^{-5}$	0.014	$6.751.10^{-5}$

response of MgB_4O_7, different proportions of Dy (0.1–1%) were added in the matrices. The results obtained via calculation and simulations were compared. For the simulations, 87 entry files were constructed using the tallies *F*6 (MeV/g per particle) and **F4* (MeV/cm^2 per particle), as described in Equations (2) and (4), and the reference material was the ICRU tissue.

2.5. Statistical analysis

The relative differences (RD) within Monte Carlo simulations and the calculated data was evaluated through Equation (5).

$$RD(\%) = \left| \frac{\left(\mu_{en}/\rho\right)_{Simulated} - \left(\mu_{en}/\rho\right)_{calculated}}{\left(\mu_{en}/\rho\right)_{calculated}} \right| \quad (5)$$

Differences between simulated and calculated data were also analyzed through the paired sample *t*-test. The purpose of the test is to determine whether there is a statistical evidence that the main difference between paired observations on a particular outcome is significantly different from zero. Data were expressed as mean value and standard error of the mean value (SEM) and the statistical differences; the significance level of $p < 0.05$ was adopted. The chi-square test (χ^2) was also used for the analysis of results. These analyses were performed using GraphPad Prism software, version 6 (GraphPad, San Diego, CA, USA).

3. Results and discussion

3.1. Calculated and simulated mass energy absorption coefficients (μ_{en}/ρ)

The calculated and simulated values of μ_{en}/ρ for Al_2O_3:C, TLD-100, MgB_4O_7, MgB_4O_7:Dy, MgB_4O_7:Dy,Li, and ICRU tissue are presented in Tables 3 and 4, respectively. In Table 3, the statistical uncertainties (type A) associated with the Monte Carlo simulation is shown, which were calculated using the relative errors of the absorbed energy of each dosimeter and the energy fluence, all provided by the MCNPX code. To obtain a statistical uncertainty below 1%, 100 million photon histories were used. For the theoretical calculations (Equation (1)), the uncertainties related to the photoionization cross section (μ/ρ) over the energy range encompassed in the data base provided by Hubbell and Seltzer are given at EPDL97 (Hubbell, 1982; Harder and Hermann, 1985). For the photon energy range of most interest in medical and biology applications, and evaluated at the present work, 0.02 MeV up to 10 MeV, the uncertainty of μ/ρ is of the order of 1%–5%. From 0.02 MeV to 0.1 MeV, the uncertainties are higher (2%) due to the higher probability of interaction such as photoionization or atomic photoeffect, and from 0.1 to 20 MeV it decreases to 1.5% (Harder and Hermann, 1985).

In Fig. 2 are shown the simulated and calculated μ_{en}/ρ values, for all of the detectors exposed to X-rays with energies from 0.02 MeV to 20 MeV. It is possible to divide this graph into two regions: below and above 0.1 MeV. The first region ($E < 0.1$ MeV) is represented by high values of μ_{en}/ρ, which is a very common behavior for TLD dosimeters, mainly for those with high Z_{eff} (Bos, 2001).

The reason for such variation in the μ_{en}/ρ is the large photon energy transfer for high Z_{eff} composites, since the photoelectric cross-section is proportional to $\sim Z^4$ (Hossain and Wagiran, 2012). The probability of photoelectric absorption increases dramatically with the atomic number of the absorber material, and decreases with increasing incident photon energy (proportional to $1/E_0^3$) (Attix, 1991). Thus, for a given absorbing material, there is generally a rapid decrease in μ_{en}/ρ when the photon energy increases (Prokic, 1986). According to Table 1, the Al_2O_3:C dosimeter has the highest Z_{eff} among all dosimeters studied in this work [$Z_{eff} = 11.28$]. Therefore, it presents the highest μ_{en}/ρ for low energies, followed by: MgB_4O_7:Dy, MgB_4O_7:Dy,Li, MgB_4O_7 [$Z_{eff} = 8.43$], TLD-100 [$Z_{eff} = 8.31$], and ICRU tissue [$Z_{eff} = 7.35$].

The μ_{en}/ρ values presented in Table 4 show good agreement with data from earlier reports in the literature (Yukihara and McKeever, 2011; Hossain and Wagiran, 2012; Gamboa et al., 1998). These μ_{en}/ρ values present the same profile for all energy range, and specially for low energies (≤ 0.1 MeV), with an abrupt increase, reaching values close to 1 cm^2/g in the case of TLD-100 and 2 cm^2/g for Al_2O_3:C (Fig. 2).

Table 4
Mass energy absorption coefficients μ_{en}/ρ (cm^2/g) calculated by Equation (1) for standard dosimeters, Al_2O_3:C and TLD-100 (LiF:Mg,Ti); Magnesium borates, MgB_4O_7, MgB_4O_7:Dy, and MgB_4O_7:Dy,Li; and ICRU tissue.

Energy	Al_2O_3:C	TLD-100 (LiF:Mg,Ti)	MgB_4O_7	MgB_4O_7:Dy (0.5%)	MgB_4O_7:Dy,Li	ICRU tissue
0.02	$1.94.10^{0}$	$6.50.10^{-1}$	$7.41.10^{-1}$	$9.57.10^{-1}$	$9.57.10^{-1}$	$5.07.10^{-1}$
0.03	$5.50.10^{-1}$	$1.83.10^{-1}$	$2.09.10^{-1}$	$2.82.10^{-1}$	$2.82.10^{-1}$	$1.44.10^{-1}$
0.04	$2.29.10^{-1}$	$7.90.10^{-2}$	$9.01.10^{-2}$	$1.23.10^{-1}$	$1.23.10^{-1}$	$6.47.10^{-2}$
0.05	$1.21.10^{-1}$	$4.55.10^{-2}$	$5.14.10^{-2}$	$6.92.10^{-2}$	$6.92.10^{-2}$	$3.99.10^{-2}$
0.06	$7.59.10^{-2}$	$3.23.10^{-2}$	$3.60.10^{-2}$	$5.88.10^{-2}$	$5.88.10^{-2}$	$3.05.10^{-2}$
0.08	$4.38.10^{-2}$	$2.39.10^{-2}$	$2.60.10^{-2}$	$4.10.10^{-2}$	$4.10.10^{-2}$	$2.53.10^{-2}$
0.1	$3.45.10^{-2}$	$2.23.10^{-2}$	$2.40.10^{-2}$	$3.36.10^{-2}$	$3.36.10^{-2}$	$2.50.10^{-2}$
0.2	$3.14.10^{-2}$	$2.48.10^{-2}$	$2.64.10^{-2}$	$2.83.10^{-2}$	$2.83.10^{-2}$	$2.94.10^{-2}$
0.3	$3.10.10^{-2}$	$2.66.10^{-2}$	$2.82.10^{-2}$	$2.90.10^{-2}$	$2.90.10^{-2}$	$3.16.10^{-2}$
0.4	$3.05.10^{-2}$	$2.73.10^{-2}$	$2.90.10^{-2}$	$2.94.10^{-2}$	$2.94.10^{-2}$	$3.25.10^{-2}$
0.5	$3.10.10^{-2}$	$2.75.10^{-2}$	$2.91.10^{-2}$	$2.94.10^{-2}$	$2.95.10^{-2}$	$3.27.10^{-2}$
0.6	$3.11.10^{-2}$	$2.74.10^{-2}$	$2.90.10^{-2}$	$2.92.10^{-2}$	$2.93.10^{-2}$	$3.25.10^{-2}$
0.8	$3.02.10^{-2}$	$2.66.10^{-2}$	$2.83.10^{-2}$	$2.85.10^{-2}$	$2.85.10^{-2}$	$3.18.10^{-2}$
1	$3.01.10^{-2}$	$2.59.10^{-2}$	$2.74.10^{-2}$	$2.75.10^{-2}$	$2.76.10^{-2}$	$3.07.10^{-2}$
1.25	$2.95.10^{-2}$	$2.47.10^{-2}$	$2.62.10^{-2}$	$2.63.10^{-2}$	$2.63.10^{-2}$	$2.94.10^{-2}$
1.5	$2.91.10^{-2}$	$2.17.10^{-2}$	$2.50.10^{-2}$	$2.51.10^{-2}$	$2.51.10^{-2}$	$2.81.10^{-2}$
2	$2.68.10^{-2}$	$1.91.10^{-2}$	$2.30.10^{-2}$	$2.31.10^{-2}$	$2.32.10^{-2}$	$2.58.10^{-2}$
3	$2.37.10^{-2}$	$1.73.10^{-2}$	$2.02.10^{-2}$	$2.03.10^{-2}$	$2.04.10^{-2}$	$2.26.10^{-2}$
4	$2.10.10^{-2}$	$1.62.10^{-2}$	$1.84.10^{-2}$	$1.85.10^{-2}$	$1.86.10^{-2}$	$2.04.10^{-2}$
5	$2.05.10^{-2}$	$1.53.10^{-2}$	$1.72.10^{-2}$	$1.73.10^{-2}$	$1.73.10^{-2}$	$1.89.10^{-2}$
6	$1.90.10^{-2}$	$1.50.10^{-2}$	$1.63.10^{-2}$	$1.64.10^{-2}$	$1.64.10^{-2}$	$1.79.10^{-2}$
8	$1.85.10^{-2}$	$1.42.10^{-2}$	$1.51.10^{-2}$	$1.53.10^{-2}$	$1.53.10^{-2}$	$1.64.10^{-2}$
10	$1.79.10^{-2}$	$1.35.10^{-2}$	$1.44.10^{-2}$	$1.46.10^{-2}$	$1.46.10^{-2}$	$1.55.10^{-2}$
15	$1.72.10^{-2}$	$1.26.10^{-2}$	$1.35.10^{-2}$	$1.37.10^{-2}$	$1.37.10^{-2}$	$1.42.10^{-2}$
20	$1.69.10^{-2}$	$1.22.10^{-2}$	$1.31.10^{-2}$	$1.33.10^{-2}$	$1.33.10^{-2}$	$1.37.10^{-2}$

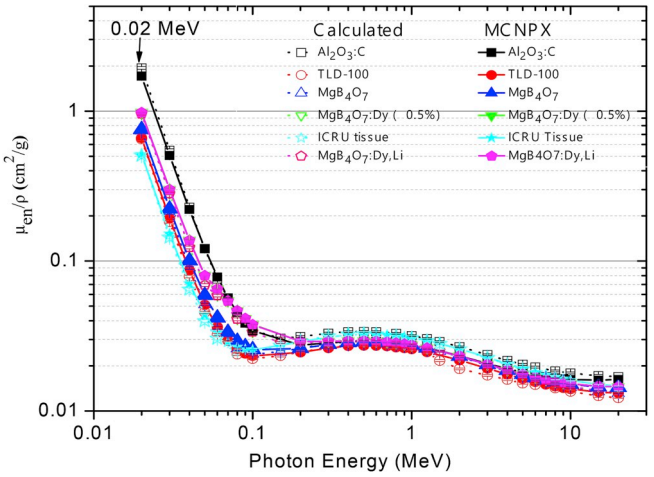

Fig. 2. Mass energy absorption coefficients (μ_{en}/ρ) for standard dosimeters, Al_2O_3:C and TLD-100 (LiF:Mg,Ti); magnesium borates, MgB_4O_7, MgB_4O_7:Dy, and MgB_4O_7:Dy,Li; and ICRU tissue simulated by MCNPX and calculated.

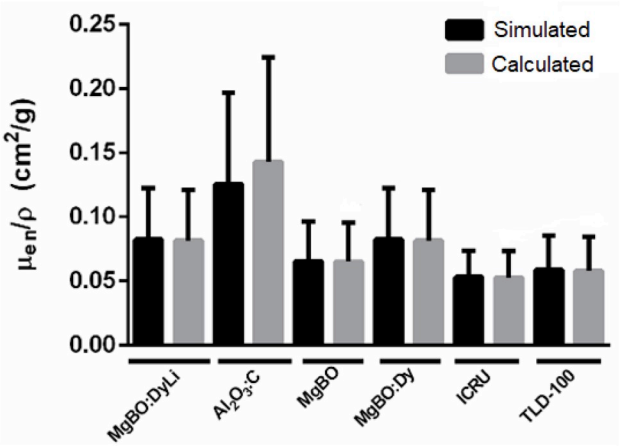

Fig. 3. Bar chart with the differences for simulated and calculated μ_{en}/ρ values of all materials. The data are expressed as mean value ± standard deviation.

For the second region (E > 0.1 MeV), decreasing μ_{en}/ρ values are observed for all compounds. For irradiation in this energy range, there is a predominance of photon interactions through the Compton Effect, with the probability being proportional to Z (Knoll, 2010). In addition, the bar chart at Fig. 3 shows that the calculated and simulated μ_{en}/ρ results are consistent between them, for most of the analyzed dosimeters.

The relative differences between simulated and calculated μ_{en}/ρ values are shown in Table 5, and the most significant RD (%) was obtained for Al_2O_3:C, with a maximum difference of 16%, at 0.2 MeV. The lack of agreement observed in this case, especially for lower energies (≤0.2 MeV), may be due to the different parameters considered (e.g. cross sections for energy deposition and irradiation scenarios) when defining μ_{en}/ρ through calculations and simulations.

For the μ_{en}/ρ values from the tables of Hubbell and Seltzer available at NIST website the energy deposition was taken into account through: fluorescence radiation (characteristic X-rays) emitted per absorbed photon; Compton-scattered photon (incoherent scattering) and radiation quanta from the annihilation of positrons (assumed to have come to rest) originating in the initial pair- and triplet-production interactions. Indeed, the complete cascade of fluorescence emission after ionization events, due to the mentioned interactions, in atomic subshells (Hubbell and Seltzer, 1995). These calculations also depart from simple Bragg additivity due to chemical-binding, phase, and density effects, as reflected in the choice of the mean excitation energy and density, for the medium.

On the other hand, the cross sections for energy deposition in the media is not available to the users, for the MNCPX (Library – ENDF/B-VI8) case, and so a more straightforward comparison related to the interactions considered by each model (Calculated and Simulated) is a complicated task. Moreover, for the simulation irradiation scenario some simplifying hypothesizes were considered such as detector dimensions, focal distance from the irradiation source and beam

Table 5
RD (%) between simulated and calculated μ_{en}/ρ values.

Energy (MeV)	Al_2O_3:C	TLD-100 (LiF:Mg,Ti)	MgB_4O_7	MgB_4O_7:Dy (0.5%)	MgB_4O_7:Dy,Li	ICRU tissue
0.02	14.65	0.26	0.42	1.13	1.03	0.68
0.03	14.13	0.10	0.85	1.23	1.14	1.55
0.04	13.88	0.49	0.98	1.37	1.28	2.15
0.05	13.73	0.43	0.93	1.24	1.16	1.97
0.06	13.44	0.45	0.94	3.17	3.09	1.83
0.08	14.03	0.13	0.59	2.25	2.19	1.07
0.1	14.77	0.07	0.12	1.41	1.36	0.69
0.2	16.00	0.11	0.26	0.25	0.27	0.13
0.3	8.88	0.05	0.01	0.49	0.51	0.24
0.4	4.69	0.14	0.14	0.44	0.46	0.18
0.5	5.87	0.03	0.14	0.30	0.65	0.22
0.6	6.76	0.08	0.03	0.30	0.66	0.43
0.8	4.77	0.55	0.16	0.39	0.40	0.37
1	9.27	0.02	0.15	0.14	0.51	0.63
1.25	12.01	0.22	0.15	0.21	0.22	0.45
1.5	15.54	8.30	0.34	0.06	0.07	0.44
2	15.09	8.23	0.63	0.21	0.23	0.77
3	14.62	8.21	0.96	0.56	0.05	0.77
4	9.95	7.65	1.38	1.03	0.48	1.32
5	13.41	6.73	1.60	1.32	1.30	1.61
6	9.25	3.89	2.11	1.89	1.87	1.37
8	11.38	2.67	3.32	2.61	2.58	2.18
10	10.19	3.61	4.24	3.63	3.59	2.68
15	7.31	5.66	6.40	6.00	5.97	4.60
20	5.62	6.15	6.43	2.31	5.00	2.14

Table 6
Statistical analyses using paired sample "T-Test" for μ_{en}/ρ simulated and calculated data (standard error of the mean value (SEM), χ^2, and p-value).

Materials	Mean ± SEM	χ^2	p-value
Al_2O_3:C	$(1.739 \pm 1.043).10^{-2}$	0.112	0.102
TLD-100 (LiF:Mg,Ti)	$(1.468 \pm 1.507).10^{-4}$	0.063	0.226
MgB_4O_7	$(3.333 \pm 15.100).10^{-5}$	0.002	0.106
MgB_4O_7:Dy (0.5%)	$(9.318 \pm 4.683).10^{-4}$	0.109	0.059
MgB_4O_7:Dy,Li	$(7.875 \pm 4.920).10^{-4}$	0.100	0.123
ICRU tissue	$(1.975 \pm 3.189).10^{-5}$	0.0001	0.951

collimation. These details are not available in the tables of Hubbell and Seltzer (1995).

For the other detectors, there is a good agreement between the calculated and simulated values, with a maximum RD of 8.3% for TLD-100 and 6.4% for MgB_4O_7. The lower RD (%) seen in the MgB_4O_7 cases lead one to believe that the complexity of interactions is increased with the Z_{eff}, reflecting on the μ_{en}/ρ estimations.

As can be seen in Table 6, all the *p-values* are larger than the significance level $p > 0.05$, and thus it may be concluded that the differences are not statistically significant. The bar chart at Fig. 3, also indicates a good agreement among the simulated and calculated data, corroborating the statistical analyses with *t*-test. The χ^2 values obtained in the present work were far below the "critical" value which is 1.96, for a degree of freedom (df) of 23, and also the highest chi–square value ($\chi^2 = 0.1123$) was presented by the Al_2O_3:C (Table 4), corroborating the results presented at the bar chart (Fig. 4).

3.2. Energy responses of TLD [S(E)]

The calculated and simulated *S*(*E*) values are shown in Fig. 4(a). The values were divided into three regions. The first one is below 0.1 MeV, the second is within 0.1 MeV–10 MeV, and the last range has energy values above 10 MeV. It can be seen that the first region (E < 0.1 MeV) is represented by strong energy responses. As the relative energy response is the ratio of the μ_{en}/ρ of the TLD and the ICRU tissue, the ideal situation is when all the values of energy response are as close as

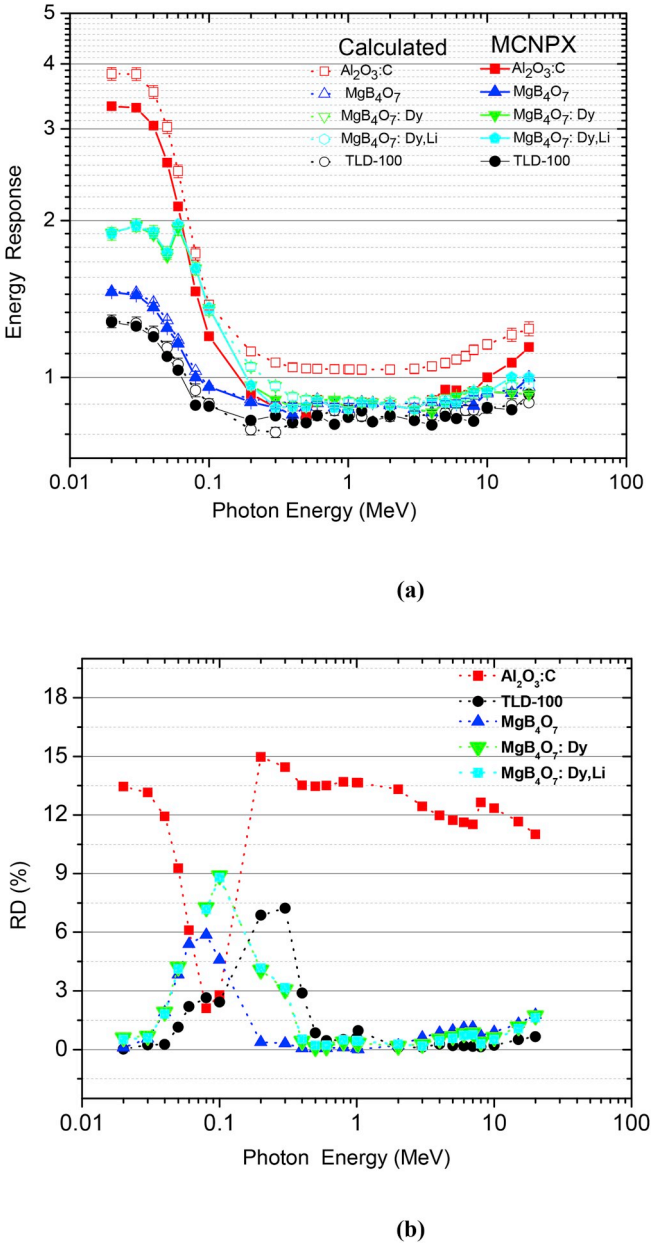

Fig. 4. (a). Energy response, *S*(*E*), achieved by simulations (MCNPX) and theoretical calculations for the borates (MgB_4O_7; MgB_4O_7:Dy and MgB_4O_7:Dy,Li) and standard TLDs (Al_2O_3:C and TLD-100) from 0.02 MeV to 20 MeV photon energy. **(b)** Relative difference, RD (%), between calculated and simulated values.

possible to unity and thus there is no variation in energy response for a broad range of energy values (Bos, 2001). The error bars, which are barely visible for the simulations case, at S (E) values, were calculated using the propagation of uncertainty from simulated and calculated μ_{en}/ρ. The uncertainties resulting from theoretical calculations were higher than those from simulated data for all the energy range, with a maximum of 3% for theoretical calculations and 0.6% for the simulation case.

Among all evaluated detectors, the Al_2O_3:C also presented the highest energy response. The results are in accordance with literature (Yukihara and McKeever, 2011), once that Al_2O_3:C has a well-known over-response (30–40%) to kiloelectron volt X-rays energies due to its high Z_{eff}, resulting in an increased probability of a photoelectric effect (Bos, 2001; Akselrod et al., 1990; C.S, 2009). This behavior was not only seen experimentally, but indeed via Monte Carlo simulations, at a

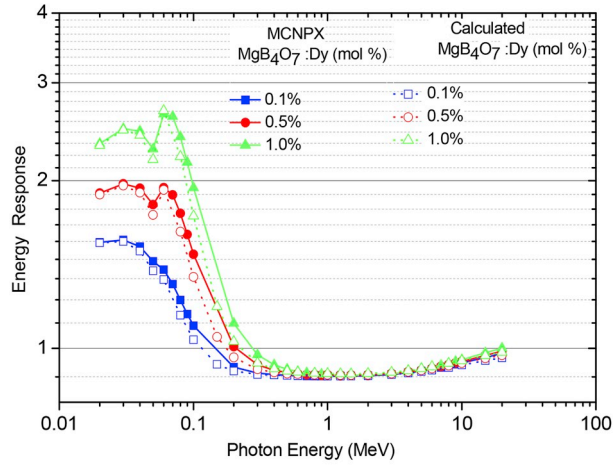

(a)

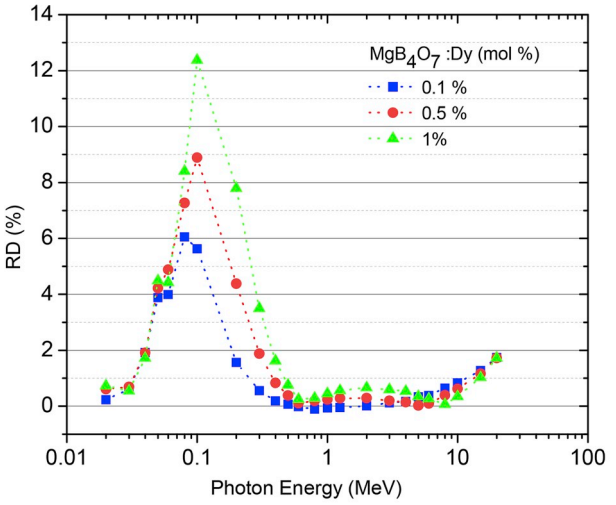

(b)

Fig. 5. (a). Effect of dopant concentration (Dy) on the energy response values of MgB_4O_7:Dy for photon energies from 0.02 MeV to 20 MeV (calculated and simulated by MCNPX). **(b).** Relative difference, RD (%), between calculated and simulated values.

previous work an overresponse of 40% was obtained for low energy X-rays cases (Mobit et al., 2006). The overresponse seen for the calculated and simulated values in the present work was approximately 33 and 40%, respectively.

At Fig. 4(b) the RD (%) is presented between the calculated and simulated energy responses. Al_2O_3:C presented the highest degree of deviation among all the detectors, with maximum RD of 15%. In this case, the graphs also show a decrease in RD (%) between 0.04 MeV and 0.1 MeV, with values reaching 2%, which represents a rough agreement between the simulated and calculated values. Above 0.1 MeV the RD % increases abruptly to 15% and shows a slow decrease reaching values of 10% at 20 MeV.

TLD-100 presented the lowest energy dependence among all the detectors evaluated, and the maximum divergence between the calculated and simulated $S(E)$ was 7%, at 0.3 MeV (Fig. 4(b)). The $S(E)$ for TLD-100 has been reported in several works and the values presented in this study are consistent with those of the literature (C.S, 2009). Olko et al. (2002) noted that 10% of the over-response of LiF:Mg,Ti exposed to X-rays in the energy range between 0.02 MeV and 0.2 MeV can be explained by an ionization density effect (Horowitz, 1981). Endres et al. (1970) obtained $S(E)$ values of 1.2 and 1.4 for TLD-100 chips and powder, respectively, when irradiated with X-rays, from 0.02 MeV to 0.05 MeV, which is a clear indication of a material-dependent ionization density effect.

The energy responses of MgB_4O_7 deviates 15% from unity. For MgB_4O_7:Dy and MgB_4O_7:Dy,Li, the energy response values are very similar and had a 20% of deviation from the unit (Fig. 4(a)). The introduction of 0.5 mol % of Dy, at MgB_4O_7 matrix, increased its energy response in 5%. The highest RD observed for MgB_4O_7 was 6%, at 0.08 MeV, and the RDs were very similar for MgB_4O_7:Dy and MgB_4O_7:Dy,Li, with maximum values of 9%, at 0.1 MeV. The results showed that the introduction of Li as a codopant, with concentration of 0.01% by total weight of MgB_4O_7, did not cause any significant change in μ_{en}/ρ, Z_{eff} and consequently to the energy response behavior of this matrix.

The second region observed in Fig. 4(a) is represented by the lowest relative energy response values, with $S(E)$ values closer to each other and to unity. In these regions, with exception of the Al_2O_3:C simulated S (E), the matrices presented a slight sub-response ($\sim$10%). In this region there is a good agreement between the simulated and calculated values of $S(E)$, for all the borates; the graph shows that RD strongly decreases above 0.1 MeV, reaching values of 1%. Above 0.3 MeV, TLD-100 also presents the same decreasing pattern in the RD (%) values, reaching very low differences ($\sim$1%). In the third region (E $>$ 10 MeV), the $S(E)$ calculated and simulated values presented a good agreement for the borates and TLD-100 (RD $<$ 2%), and still a large RD (%) for the Al_2O_3:C case ($\sim$16%).

3.3. Effects of dopant concentration on the energy response of MgB_4O_7

In Fig. 5(a), the effect of Dy concentration on the calculated and simulated energy response values for MgB_4O_7:Dy can be seen. In this figure it is possible to observe an increase in the energy dependence with the dopant concentration at low kiloelectron volt range ($<$ 0.1 MeV). For example, at 0.05 MeV the energy response of MgB_4O_7:Dy (1%) is 50% higher when compared to MgB_4O_7:Dy (0.1%). Indeed at 50 keV, the K-edge absorption of Dy is incremented with the concentration of this dopant.

The RD (%) between the simulated and calculated $S(E)$ values was high at K-edge absorption regions ($0.04 < E_{k\text{-}edge} < 0.1$ MeV), and these values increased with the dopant concentration, as seen at Fig. 5(b). At 0.1 MeV, the RD was 12%, 9% and 5% for MgB_4O_7:Dy (1%), MgB_4O_7:Dy (0.5%) and MgB_4O_7:Dy (0.1%), respectively. The discrepancies of values and high uncertainties of μ/ρ at the vicinity of absorption edge are related to effects of molecular and ionic chemical binding which increases the complexity of interactions at these regions (Hubbell, 1999). For higher energies, the $S(E)$ presented a decreasing pattern, and above 0.3 MeV all the RDs, regardless of dopant concentration, are below 2%.

It is already known that for the MgB_4O_7 matrix, the increase in dopant concentration raises the detector sensitivity until a certain point (Souza et al., 2015). Nevertheless, from the results shown here, it can be seen that the concentration also increases the energy dependence effects, and such behavior should be taken into account for applications at low photon energy range. For higher energy range, the concentration effect was negligible for this matrix.

4. Conclusions

The μ_{en}/ρ and relative energy response values of MgB_4O_7, MgB_4O_7:Dy, and MgB_4O_7:Dy,Li using Monte Carlo simulations and calculated data were obtained in this work. It was observed that the μ_{en}/ρ and energy responses of the materials were higher in the low energy range (E $<$ 100 keV), which is related to the strong interaction of radiation with matter through photoelectric absorption. The values of μ_{en}/ρ and relative energy response for the compounds studied were also compared with those of commercial TLDs, such as TLD-100 and Al_2O_3:C, and with ICRU tissue data for the same energy range. The

results showed that the highest values of μ_{en}/ρ and relative energy response were obtained for Al_2O_3:C, followed by MgB_4O_7:Dy, MgB_4O_7:Dy,Li, MgB_4O_7, TLD-100 and ICRU tissue.

Although the tables of Hubbell and Seltzer (1995) are known as reference for estimation of the dosimetric quantity μ_{en}/ρ, it was difficult to perform more straightforward comparisons with simulated results, due to the lack of information regarding the irradiation scenario (e.g. detector dimensions and position, source to surface distance, and beam collimation) of the tables. On the other hand, it is not possible for the MCNPX user to access the cross-section interaction considered by the code, which is very well described in the tables of Hubbel and Seltzer. For the detectors evaluated, except Al_2O_3:C, the calculations and the simulations matched well for the μ_{en}/ρ and relative energy responses, with RD below 9%. For Al_2O_3:C there is a lack of agreement among these values and the RD % reached values of 16%; these differences are seen mainly in low photons energy range, and it is highlighted due to the high Z_{eff} presented by the Al_2O_3:C.

It was also observed that as the Dy concentration in the MgB_4O_7 matrix increases, the relative energy response of the TLD also increases. For the low energy region, an increase in the photon energy occurs and there is a reduction in energy response, although at around 50 keV there is an abrupt increase in the absorption, increasing the relative energy response of MgB_4O_7. This fact is directly related to the K-edge absorption, due to the high Z of the dopant. It was also observed that the addition of Li as a codopant did not change the μ_{en}/ρ or relative energy response curves, due to its low concentration.

Overall, a good agreement was shown in the present work between the calculated and simulated data for μ_{en}/ρ estimation for several TLDs used in radiation dosimetry. So, the Monte Carlo code can be used with reliability to estimate the μ_{en}/ρ for MgB_4O_7 doped with different concentrations of Dy, and when co-dopants are added to its matrix.

Acknowledgments

The authors are thankful to the Brazilian Research Support Agencies, FAPITEC/SE, CAPES, CNPq (301305/2016-8 and 308090/2016-0), and CNEN.

References

Akselrod, M.S., Kortov, V.S., Kravetsky, D.J., Gotlib, V.I., 1990. Highly sensitive thermoluminescent anion-defective alpha-Al_2O_3:C single crystal detectors. Radiat. Prot. Dosim. 32, 15–20. https://doi.org/10.1093/oxfordjournals.rpd.a080715.

Attix, F.H., 1991. Introduction to Radiological Physics and Radiation Dosimetry. Wiley Interscience, Madison, USA.

Bos, A.J.J., 2001. High sensitivity thermoluminescence dosimetry. Nucl. Inst. Meth. Phys. Res B. 184, 3–28. https://doi.org/10.1016/S0168-583X(01)00717-0.

Chen, R., McKeever, S.W.S., 1997. Theory of Thermoluminescence and Related Phenomena. World Scientific, New Jersey, USA.

Reft, C.S., 2009. The energy dependence and dose response of a commercial optically stimulated luminescent detector for kilovoltage photon, megavoltage photon, and electron, proton, and carbon beams. Med. Phys. 36, 1690–1699. https://doi.org/10.1118/1.3097283.

Endres, G.W.R., Kathren, R.L., Kocher, F., 1970. Thermoluminescence personnel dosimetry at Hanford – II. Energy dependence and application of TLD materials in operational health physics. Health Phys. 18, 665–672.

Gamboa, B., Buen, A.E., Ruiz, C.G., Villafuerte, M.R., Flores, A., Brandan, M.E., 1998. Thermoluminescent response and relative efficiency of TLD-100 exposed to low-energy x-rays. Phys. Med. Biol. 43, 2073–2083. https://doi.org/10.1088/0031-9155/43/8/006.

Harder, D., Hermann, K.P., 1985. Tissue equivalent materials and ICRU sphere. Radiat. Prot. Dosim. 12, 125–128. https://doi.org/10.1093/oxfordjournals.rpd.a079496.

Horowitz, Y.S., 1981. The theoretical and microdosimetric basis of thermoluminescence and applications to dosimetry. Phys. Med. Biol. 26, 765–824.

Hossain, I., Wagiran, A.H., 2012. Mass energy absorption coefficients for 0.2–20 MeV photon in Ge-doped optical fiber and TLD-100 by Monte Carlo n-particle code version 5 (MCNP5). Optoelectron Adv. Mater. Rapid. Commun. 6, 162–164.

Hubbell, J.H., 1982. Photon mass attenuation and energy absorption coefficients for 1 keV to 20 MeV. Int. J. Appl. Radiat. Isot. 33, 1269–1290. https://doi.org/10.1016/0020-708X(82)90248-4.

Hubbell, J.H., 1999. Review of photon interaction cross section data in the medical and biological context. Phys. Med. Biol. 44 (1), R1–R22.

Hubbell, J.H., 2000. X-ray cross-sections and crossroads (the international radiation physics society) – Richard Pratt's contributions to both. Radiat. Phys. Chem. 59, 113–125. https://doi.org/10.1016/S0969-806X(00)00281-4.

Hubbell, J.H., Seltzer, S.M., 1995. Tables of X-Ray Mass Attenuation Coefficients and Mass Energy-Absorption Coefficients from 1 keV to 20 MeV for Elements Z = 1 to 92 and 48 Additional Substances of Dosimetric Interest, NISTIR Report 5632. NIST, Gaithersburg, USA.

ICRU-33, 1980. International Commission on Radiation Units and Measurements: Radiation Quantities and Units. ICRU Report 33. International Commission on Radiation Units and Measurements, Bethesda, USA.

Knoll, G.F., 2010. Radiation Detection and Measurement, fourth ed. Wiley E-Text, EUA.

Kumar, T.K., Reddy, K.V., 1997. Effective atomic numbers for materials of dosimetric interest. Radiat. Phys. Chem. 50, 545–553. https://doi.org/10.1016/S0969-806X(97)00089-3.

Manjunatha, H.C., 2014a. Comparison of effective atomic numbers of the cancerous and normal kidney tissue. Radiat. Protec. Environ. 38, 83–91. https://doi.org/10.4103/0972-0464.169376.

Manjunatha, H.C., 2014b. A study of photon interaction parameters in lung tissue substitutes. J. Med. Phys. 39, 112–115. https://doi.org/10.4103/0971-6203.131286.

Manjunatha, H.C., 2016. Mass attenuation coefficient and its photon interaction derivables of some skeletal muscle relaxants. J. Rad. Cancer. Res. 7, 18–26. https://doi.org/10.4103/0973-0168.184608.

Manjunatha, H.C., Rudraswamy, B., 2011. Computation of CT-number and Zeff in teeth. Health Phys. 100, S92–S99. https://doi.org/10.1097/HP.0b013e3181f508ac.

Manjunatha, H.C., Rudraswamy, B., 2012. Photon interaction parameters of dosimetric interest in bone. Health Phys. 10, 322–329. https://doi.org/10.1097/HP.0b013e3182585a5b.

Manjunatha, H.C., Rudraswamy, B., 2013. Study of effective atomic number and electron density for tissues from human organs in the energy range of 1 keV–100 GeV. Health Phys. 104, 158–162. https://doi.org/10.1097/HP.0b013e31827132e3.

McKeever, S.W.S., 1985. Thermoluminescence of Solids. Cambridge Solid State Science Series, UK: Cambridge.

Mobit, P.N., Nahum, A.E., Mayles, P.A., 1998. A Monte Carlo study of the quality dependence factors of common TLD materials in photon and electron beams. Phys. Med. Biol. 43, 2015–2032. https://doi.org/10.1088/0031-9155/43/8/002.

Mobit, P., Agyingi, E., Sandison, G., 2006. Comparison of the energy-response factor of LiF and Al_2O_3 in radiotherapy beams. Radiat. Prot. Dosim. 119, 497–499. https://doi.org/10.1093/rpd/nci676.

Olko, P., Bilski, P., Kim, J.L., 2002. Microdosimetric interpretation of the photon energy dependence of Lif:Mg,Ti detectors. Radiat. Prot. Dosim. 100, 119–122. https://doi.org/10.1093/oxfordjournals.rpd.a005826.

Paluch-Ferszt, M., Kozłowska, B., Souza, S.O., Souza, L.F., Souza, D.N., 2014. Analysis of dosimetric peaks of MgB4O7:Dy (40% Teflon) versus LiF:Mg,Ti TL detectors. Nukleonika 61 (1), 49–52. https://doi.org/10.13140/RG.2.1.2083.4965.

Pelowitz, D.B., 2011. MCNPX User's Manual, Version 2.7.0. Report LA-CP-11-00438. Los Alamos National Laboratory, USA.

Prokic, M., 1983. MgB_4O_7:Mn as a new TL dosemeter. Radiat. Prot. Dosim. 47, 191–193. https://doi.org/10.1093/oxfordjournals.rpd.a081730.

Prokic, M., 1986. Magnesium borate in TL dosimetry. Radiat. Prot. Dosim. 17, 393–396. https://doi.org/10.1093/oxfordjournals.rpd.a079845.

Prokic, M., 2000. Effect of lithium co-dopant on the thermoluminescence response of some phosphors. Appl. Radiat. Isot. 52, 97–103.

Prokic, M., 2007. Individual monitoring based on magnesium borate. Radiat. Prot. Dosim. 125, 247–250. https://doi.org/10.1093/rpd/ncl116.

Prokic, M., Botter, J., 1993. Comparison of main thermoluminescent properties of some TL dosimeters. Radiat. Prot. Dosim. 47, 185–199. https://doi.org/10.1093/oxfordjournals.rpd.a081731.

Singh, V.P., Badiger, N.M., 2013. Photon energy absorption buildup factors of gaseous mixtures used in radiation detectors. Int. J. Radio. Prot. 48, 63–78.

Souza, L.F., Vidal, R.M., Souza, S.O., Souza, D.N., 2014. Thermoluminescent dosimetric comparison for two different MgB_4O_7:Dy production routes. Radiat. Phys. Chem. 104, 100–103. https://doi.org/10.1016/j.radphyschem.2014.04.036.

Souza, L.F., Antonio, P.L., Caldas, L.V.E., Souza, D.N., 2015. Neodymium as a magnesium tetraborate matrix dopant and its applicability in dosimetry and as a temperature sensor. Nucl. Instr. Meth. Phys. Res. A 784, 9–13. https://doi.org/10.1016/j.nima.2014.12.030.

Turner, J.E., 1995. Atoms, Radiation and Radiation Protection, second ed. Wiley, New York, USA.

Wang, B., Kim, C.H., Xua, X.G., 2004. Monte Carlo modeling of a high-sensitivity MOSFET dosimeter for low- and medium-energy photon sources. Med. Phys. 31, 1003–1008. https://doi.org/10.1118/1.1688272.

Yukihara, E.G., McKeever, S.W.S., 2011. Optically Stimulated Luminescence, Fundamentals and Applications. John Wiley & Sons, Oklahoma, USA.

Yukihara, E.G., Milliken, E.D., Oliveira, L.C., Orante-Barro, V.R., Jacobsohn, L.G., Blair, M.W., 2013. Systematic development of new thermoluminescence and optically stimulated luminescence materials. J. Lumin. 133, 203–210. https://doi.org/10.1016/j.jlumin.2011.12.018.

Yukihara, E.G., Milliken, E.D., Doull, B., 2014. Thermally stimulated and recombination processes in MgB_4O_7 investigated by lanthanide doping. J. Lumin. 154, 251–259. https://doi.org/10.1016/j.jlumin.2014.04.038.

Yukihara, E.G., Doull, B.A., Gustafson, T., Oliveira, L.C., Kurt, K., Milliken, E.D., 2017. Optically stimulated luminescence of MgB_4O_7:Ce,Li for gamma and neutron dosimetry. J. Lumin. 183, 525–532. https://doi.org/10.1016/j.jlumin.2016.12.001.